scientific reports

Check for updates

OPEN

WTAP-dependent N6-methyladenosine methylation of lncRNA TEX41 promotes renal cell carcinoma progression

Zhenwei Zhou[1,2], Xianjiong Chen[1,2], Huan Wang[1], Lifeng Ding[1], Mingchao Wang[1], Gonghui Li[1]✉ & Liqun Xia[1]✉

The methyltransferase Wilms' tumor 1-associated protein (WTAP) has been reported to be dysregulated in various tumors. However, its role in renal cell carcinoma (RCC) remains elusive. Here, we explored whether WTAP was upregulated in RCC specimens compared to normal tissues. Functionally, WTAP promoted RCC cell proliferation and metastasis in vivo and in vitro. Mechanistically, WTAP act as an N6-methyladenosine transferase to regulate the m^{6}A modification of long noncoding RNA TEX41. Then, the upregulated m^{6}A modification destabilized TEX41 in a YTHDF2-dependent manner. Furthermore, TEX41 interacted with the SUZ12 protein and increased the histone methyltransferase activity of SUZ12, resulting in HDAC1 silencing. Totally, our study demonstrated the oncogenic the role of WTAP/TEX41/SUZ12/HDAC1 axis in RCC progression.

Keywords WTAP, TEX41, Renal cell carcinoma, HDAC1

Abbreviations

WTAP	Wilms tumor 1-associated protein
RCC	Renal cell carcinoma
ccRCC	Clear cell RCC
pRCC	Papillary RCC
chRCC	chromophobe RCC
m^{6}A	N6-methyladenosine
FBS	Fetal bovine serum
PRC2	Polycomb represssor complex 2

Renal cell carcinoma (RCC) is the most common lethal malignancy worldwide[1]. There are more than 400,000 patients diagnosed with RCC annually, and nearly two-thirds of the patients are male[1,2]. Histologically, RCC contains three major subtypes, including clear cell RCC (ccRCC), papillary RCC, and chromophobe RCC, whereas another subtypes account for less than 1% [3,4]. Regrettably, nearly 30% of RCC patients had metastases when first diagnosed[5]. Consequently, it is urgent to determine the underlying mechanism of RCC proliferation and metastasis[6]. However, few studies focused on the epigenetic alteration in RCC.

N6-methyladenosine (m^{6}A) modification is the most abundant post-transcriptional modification in various types of RNAs, including mRNA, tRNA, rRNA, and noncoding RNA (ncRNA)[7,8]. Generally, m^{6}A modification affects RNA stability, splicing, translocation, and translation[9]. Recent studies have shown that several m^{6}A modification writers and erasers are involved in RCC progression[10]. m^{6}A writers, including METTL3, METTL14, and WTAP, and m^{6}A eraser FTO have been reported to regulate ccRCC development via regulating the m^{6}A modification level of mRNA[11–14]. However, it is still unknown how WTAP-regulated long ncRNA (lncRNA) contributes to RCC progression.

In this study, WTAP was identified upregulated in renal cell carcinoma tissues compared to normal tissues. Functional assays showed that WTAP promoted RCC proliferation and metastasis in vivo and in vitro. MeRIP-seq revealed that the m^{6}A modification of lncRNA TEX41 decreased with WTAP knockdown, which increased the stability of TEX41. RNA pull-down assay followed by mass spectrometry identified that SUZ12 could interact with TEX41. Particularly, this interaction increased the histone methyltransferase activity of SUZ12, resulting in

[1]Department of Urology, Sir Run Run Shaw Hospital, Zhejiang University School of Medicine, Hangzhou 310016, China. [2]Zhenwei Zhou and Xianjiong Chen contributed equally. ✉email: 3193119@zju.edu.cn; xialiqun@zju.edu.cn

HDAC1 silencing. Overall, our study provides the role of WTAP/TEX41/SUZ12/HDAC1 in RCC, which could be the potential therapeutic target for RCC treatment.

Results

WTAP is upregulated in RCC

To identify WTAP expression level in RCC, we analyzed the expression of WTAP in TCGA-KIRC database using UALCAN database (https://ualcan.path.uab.edu/index.html), the result showed that WTAP increased in tumor samples compared to normal samples (Fig. 1A). Then, WTAP was approved upregulated in mRNA and

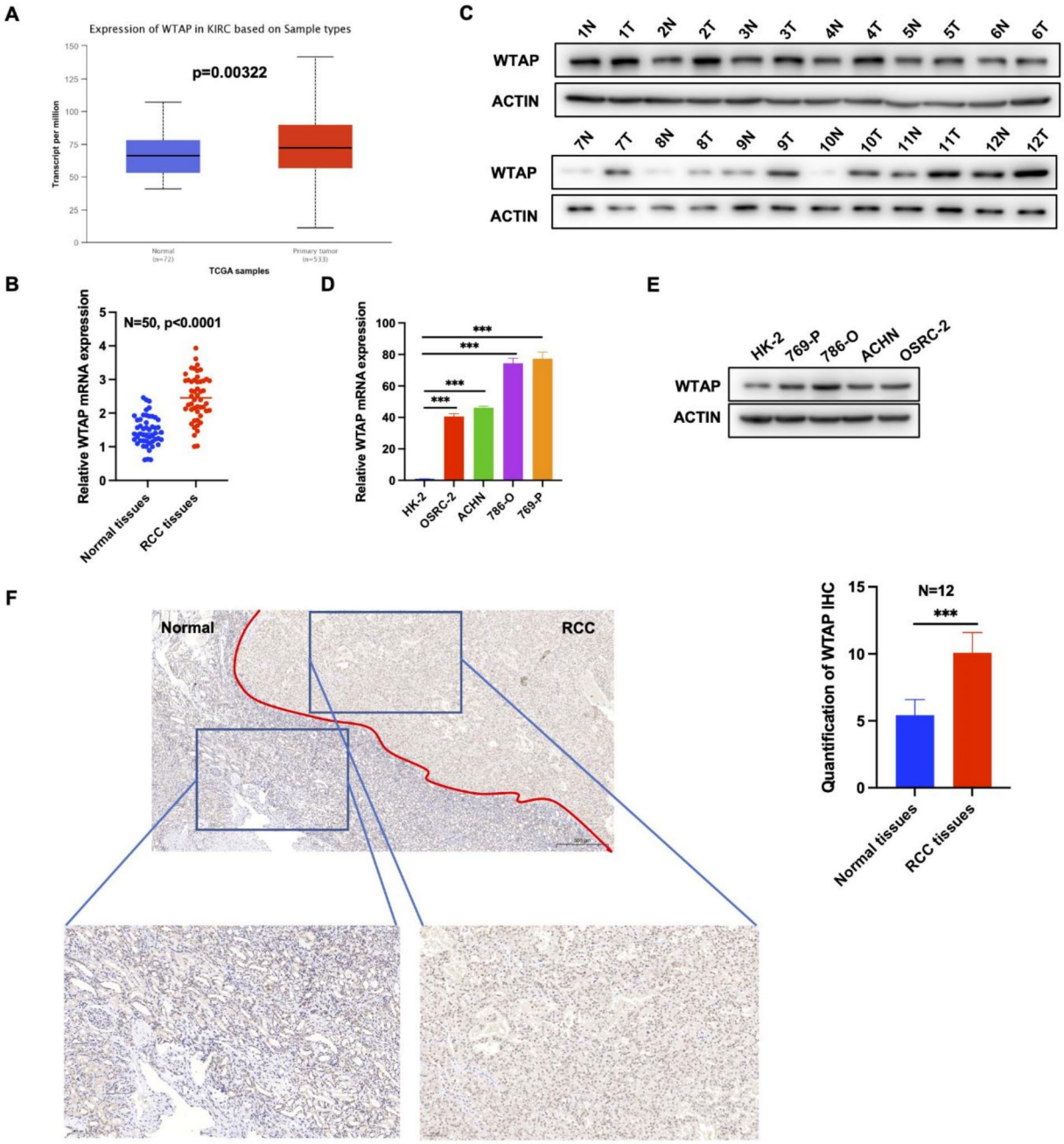

Fig. 1. WTAP is upregulated in RCC (**A**) The relative mRNA expression of WTAP based on the data from the TCGA-KIRC database which including 72 normal samples and 533 RCC samples. (**B**) The relative mRNA expression of WTAP in 50 paired RCC tissues. (**C**) The relative protein expression of WTAP in 12 paired RCC tissues. (**D**) The relative mRNA expression of WTAP in RCC cell lines and normal cell line HK-2. (**E**) The relative protein expression of WTAP in RCC cell lines and normal cell line HK-2. (**F**) Representative images of IHC staining with WTAP in RCC and normal specimens. The experiments were repeated three times independently. Data are presented as the mean ± SD. $^{***}P < 0.001$.

protein levels in our clinical RCC samples (Fig. 1B and C). Consistently, WTAP expression level was extremely higher in RCC cell lines (769-P, 786-O, ACHN, and OSRC-2) than in the normal cell line HK-2 (Fig. 1D and E). Also, immunohistochemistry (IHC) analysis showed that WTAP was highly expressed in RCC tissues (Fig. 1F). These data indicated that WTAP was upregulated in RCC.

WTAP promotes RCC cell proliferation and metastasis

In order to understand the role of WTAP in RCC, WTAP-specific siRNAs were transfected into WTAP high-expression cell lines, including 786-O and 769-P, and WTAP overexpression plasmids were applied into the WTAP low-expression cell line, OSRC-2. The knockdown or overexpression efficiency was verified using western blotting (Fig. 2A). CCK-8 assays showed that knockdown of WTAP inhibited 786-O and 769-P cell proliferation, whereas WTAP overexpression promoted OSRC-2 cell proliferation (Fig. 2B). The colony formation assay also revealed that WTAP knockdown inhibited RCC cells proliferation, while WTAP overexpression promoted RCC cells proliferation (Fig. 2C). Since WTAP promotes RCC cell proliferation, we then assessed its role in cell cycle or apoptosis of RCC cells. Flow cytometry analysis revealed that WTAP knockdown results in the cell cycle arrest in the G1 phase, while WTAP overexpression had the opposite effect (Fig. 2D). However, manipulating the expression of WTAP had little effect on RCC cell apoptosis (Supplementary Fig. 1A and 1B). Furthermore, transwell migration and invasion assays were applied to investigate the role of WTAP in metastasis. The results showed that knockdown of WTAP restrained RCC cell migration and invasion, while overexpression of WTAP enhanced RCC cell migration and invasion (Fig. 2E). These data demonstrated that WTAP promotes RCC cell proliferation and metastasis.

WTAP destabilized lncRNA TEX41 through YTHDF2 in an m6A-dependent manner

To elucidate the regulatory role of WTAP in RCC through its m^6A methyltransferase activity, m^6A methylated RNA immunoprecipitation sequencing (MeRIP-seq) was performed in 786-O and 769-P cells with WTAP stable knockdown. The investigation of m6A peak distributions revealed that the overall patterns of m6A distribution were consistent between the control and WTAP knockdown groups (Supplementary Fig. 2A). Furthermore, analysis of the consensus motif demonstrated a high concentration at m6A sites in both control and WTAP-silenced cells (Supplementary Fig. 2B). A total of 23 hypomethylated lncRNAs ($|\log_2 FC|>1$, $p<0.05$) were shown in Venn diagram (Fig. 3A). From this initial set, 10 lncRNAs were excluded due to their absence from the TCGA database, limiting their clinical relevance. The remaining 13 lncRNAs were further evaluated based on their expression levels in RCC tissues. We selected 7 lncRNAs that exhibited significant dysregulation in RCC compared to normal kidney tissues. m^6A-RIP assay was then performed, and TEX41 was hypomethylated after WTAP knockdown in WTAP high-expression cell lines (786-O and 769-P cells) (Fig. 3B). Next, the SRAMP database was used to explore the m^6A modification site of TEX41, and three strong confident m^6A modification sites (587 A, 3927 A, and 4336 A) were predicted (Fig. 3C). We then constructed wild-type and three mutant (A-G mut) plasmids (Fig. 3D). MeRIP-qPCR assay demonstrated that the m^6A modification level decreased in cells transfected with mutant 3 plasmids (Fig. 3E), suggesting that 4336 A is the key m^6A site of TEX41. Next, we designed two 50 nt biotinylated RNA probes around the 4336 site with or without 4336 A mutant (A to G mutant), which named probe_WT and probe_Mut (Fig. 3F). Next, we performed RNA pulldown assay using these two probes. And the result showed that probe_WT could interact with WTAP, while probe_Mut cannot interact with WTAP (Fig. 3G), suggesting that 4336 A is the key m^6A site of TEX41. Next, we knockdown and overexpression of WTAP in RCC cells. Results showed that WTAP repressed the expression of TEX41 (Fig. 3H and I). We then evaluated the half-time of TEX41 in WTAP overexpression or knockdown cells treated with actinomycin D, the result showed that the half-time of TEX41 decreased in WTAP overexpression cells (Fig. 3J), while WTAP knockdown increased the half-time of TEX41 (Supplementary Fig. 2C), suggesting that WTAP affect TEX41 RNA stability.

Previous studies have revealed that m^6A readers IGF2BPs (IGF2BP1, IGF2BP2, and IGF2BP3) and YTHDF2 could influence the stability of target m^6A containing RNA in an m^6A-dependent way[15]. RIP-qPCR assays showed that YTHDF2, but not IGF2BPs, could specifically interact with TEX41 (Fig. 3K). Also, qRT-PCR assays revealed that silencing of YTHDF2 could elevate the expression of TEX41 (Fig. 3L). We proceeded to assess the half-life of TEX41 in YTHDF2 knockdown cells treated with actinomycin D, revealing an increased half-life of TEX41 in YTHDF2 knockdown cells (Fig. 3M). Furthermore, we investigated whether the interaction between TEX41 and YTHDF2 is dependent on the m6A modification of TEX41. The YTHDF2-RIP assay demonstrated that silencing WTAP impaired the interaction between YTHDF2 and TEX41 (Fig. 3N), while overexpression of WTAP enhanced this interaction (Fig. 3O). Moreover, correlation analysis showed that WTAP and TEX41 have a negative correlation in RCC samples (Fig. 3P). Totally, these data suggest that WTAP destabilized TEX41 through YTHDF2 in an m6A-dependent manner.

LncRNA TEX41 restrained RCC cells proliferation and metastasis

LncRNA TEX41 has been reported dysregulated in many tumors, such as B-Cells Acute Lymphoblastic Leukemia and melanoma[16,17]. To elucidate the expression pattern of TEX41 in RCC, we first detected the expression of TEX41 in 50 paired RCC tissues and adjacent normal tissues. The result revealed that TEX41 was downregulated in tumor specimens (Fig. 4A). Also, TEX41 was highly expressed in the normal cell line HK-2 compared to RCC cell lines (Fig. 4B). Then, we explored the role of TEX41 in RCC. TEX41 siRNAs were transfected into the TEX41 high-expression cell line, OSRC-2, and TEX41 overexpression plasmids were transfected into TEX411 low-expression cell lines, 769-P and 786-O. The knockdown or overexpression efficiency were verified using qRT-PCR (Fig. 4C and D). CCK-8 assay showed that knockdown of TEX41 promoted OSRC-2 cell proliferation, whereas overexpression of TEX41 restrained RCC cell proliferation (Fig. 4E). Transwell assays indicated that TEX41 impaired the migration and invasion abilities of RCC cells (Fig. 4F and G). Furthermore, to determine

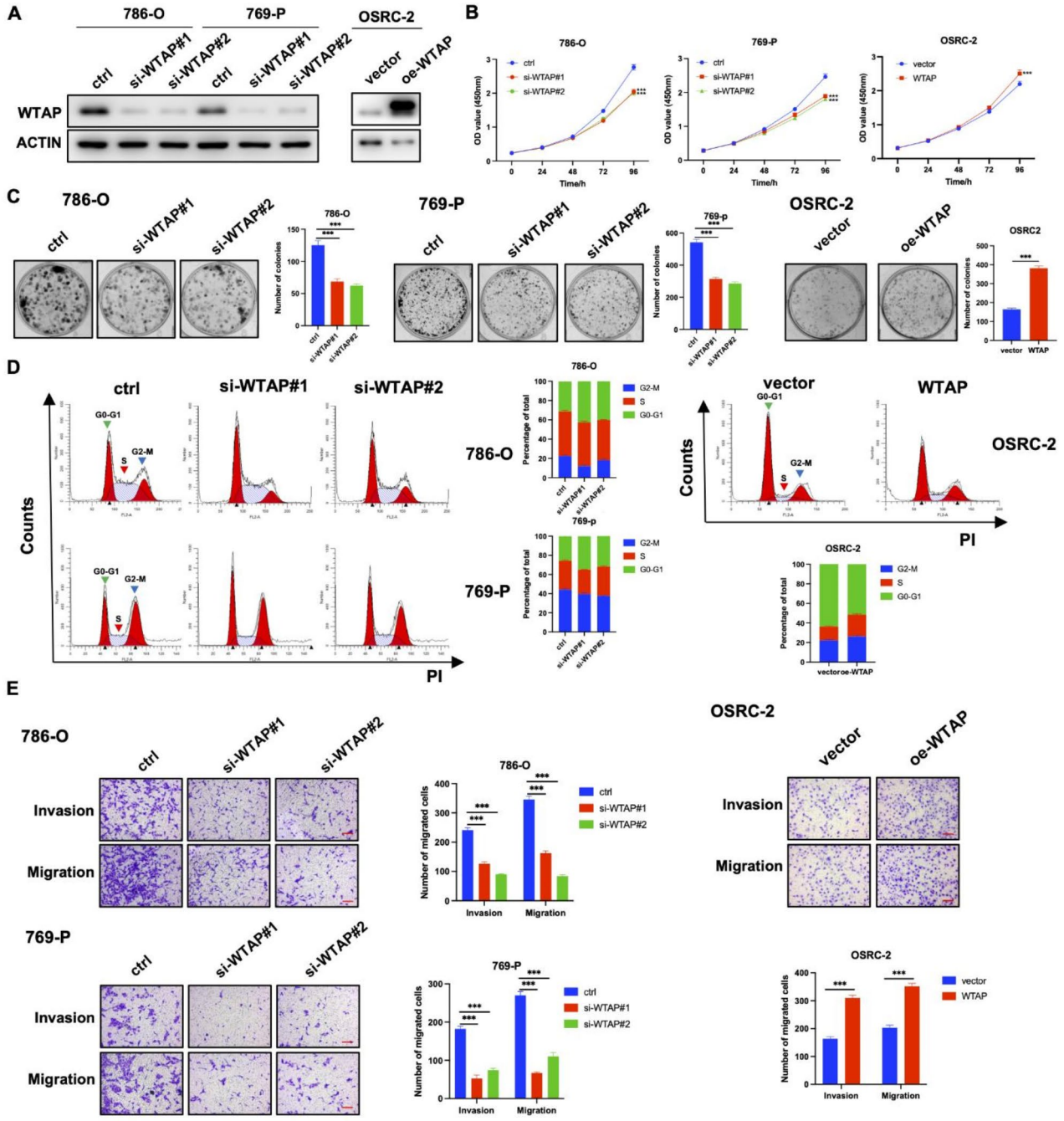

Fig. 2. WTAP promotes RCC cells proliferation and metastasis (**A**) Western blotting assays showing the WTAP knockdown or overexpression efficiency. (**B**) and (**C**) Cell proliferation was analyzed using CCK-8 (**B**) and colony formation (**C**) assays with WTAP knockdown or overexpression. (**D**) Flow cytometry detected the alteration of the cell cycle (including G0-G1, S, and G2-M phase) with WTAP knockdown or overexpression. (**E**) Cell metastatic ability was analyzed using transwell migration and invasion assays with WTAP knockdown or overexpression. Scale bars, 5 μm. The experiments were repeated three times independently. Data are presented as the mean ± SD. $^{***}P < 0.001$.

whether WTAP exerts its tumor-promoting effect through decreasing TEX41 expression, rescue assays were performed using WTAP overexpression cells with or without TEX41 overexpression. TEX41 expression was examined using qRT-PCR (Fig. 4H). CCK-8 assay showed that overexpression of TEX41 could reverse the promoting effect of WTAP in RCC cell proliferation (Fig. 4I). Transwell assay also obtained the similar results (Fig. 4J). Totally, these data reveal that TEX41 inhibits RCC cell proliferation and metastasis.

TEX41 interacted with SUZ12 in RCC cells

Various studies have demonstrated that the interaction between lncRNA and RNA binding proteins contributes to tumor progression. To explore the binding protein of TEX41, the online database catRAPID (http://service.tartaglialab.com/page/catrapid_group) was applied (date of accession: 6 May 2022) (Fig. 5A). Among the predicted proteins, SUZ12 was selected. Then, RNA pull-down, RIP-qPCR, and FISH-IF assays were used to verify the interaction between TEX41 and SUZ12 (Fig. 5B and D). Then, we detected the impact of TEX41 on SUZ12 expression. The result revealed that TEX41 have little effect on SUZ12 expression (Fig. 5E). Meanwhile, SUZ12 didn't alter the expression of TEX41 (Fig. 5F). Considering that SUZ12 is the subunit of polycomb represssor complex 2 (PRC2), which leading to the silence of target genes by methylating Lys-27 of histone 3 (H3K27me3), we detected the total H3K27me3 levels with TEX41 knockdown or overexpression. The results showed that TEX41 silencing decreased the total H3K27me3 level in RCC cells, while overexpression of TEX41 increased the total H3K27me3 level in RCC cells (Fig. 5G). Collectively, these data indicate that TEX41 could bind with SUZ12 and influence total H3K27me3 levels in RCC cells.

TEX41 modulated HDAC1 expression through regulating H3K27me3 level in its promotor region

Previous studies have revealed that PRC2 complex could regulate various gene transcription through modulating H3K27me3 levels at the target gene promotor[18,19]. Thus, we verified whether TEX41 could affect the expression of HDAC1, one of the famous downstream target of PRC2, through SUZ12[20]. Western blotting and RT-qPCR assays showed that TEX41 could regulate HDAC1 expression in mRNA and protein levels (Fig. 6A and B). Then, CHIP-qPCR assays revealed that SUZ12 was enriched in the HDAC1 gene promotor (Fig. 6C). What's more, overexpression of TEX41 increased the enrichment of SUZ12 in the HDAC1 promotor, while silencing of TEX41 decreased the enrichment of SUZ12 in the HDAC1 promotor (Fig. 6C). In addition, we detected the H3K27me3 level in HDAC1 promotor with changing TEX41 expression. The results demonstrated that TEX41 increased the H3K27me3 level in HDAC1 promotor (Fig. 6D). Since WTAP-regulated TEX41 expression as we previous verified, CHIP-qPCR assays were performed to explore the role of WTAP in regulating H3K27me3 level in HDAC1 promotor. As expected, silencing of WTAP increased the enrichment of SUZ12 and H3K27me3 level in HDAC1 promotor, while overexpression of WTAP decreased the enrichment of SUZ12 and H3K27me3 level in HDAC1 promotor (Fig. 6E and F). Furthermore, western blotting assay showed that WTAP controlled HDAC1 expression through regulating TEX41 (Fig. 6G).

HDAC1 is one of the members of histone deacetylase involved in cancer, allergic diseases, and cardiovascular diseases[21–23]. Kiweler et al. reported that HDAC1 was an oncogene that promoted renal cell carcinoma proliferation[24]. Another group revealed that HDAC1 enhanced RCC cells metastasis by increasing MMP expression[25]. Indeed, we first detected the expression HDAC1 in our 50 paried RCC specimens, the results showed that HDAC1 was upregulated in RCC tissues compared to normal tissues (Fig. 6H). Correlation analysis revealed that WTAP was positively correlated with HDAC1 in our cohort and TCGA-KIRC database (Fig. 6I and J). We further explored whether WTAP exert its oncogenic role in RCC through regulating HDAC1. CCK-8 assay demonstrated that silencing of HDAC1 reversed the promoting effect of WTAP overexpression in RCC cells (Fig. 6K). Similarly, silencing of HDAC1 reversed the promoting effect of WTAP overexpression on the metastasis ability of RCC cells (Fig. 6L). Totally, these data demonstrate that WTAP-modulated TEX41 regulates HDAC1 expression through influencing H3K27me3 level in its promotor region.

Silencing of WTAP restrained RCC progression in vivo

To further evaluate the role of WTAP on RCC proliferation in vivo, xenograft mice model was established. The results showed that WTAP knockdown restrained 769-P cell growth in vivo (Fig. 7A). Then, we detected the WTAP, TEX41, and HDAC1 expression in both control and WTAP knockdown group. The results showed that both WTAP and HDAC1 were downregulated in the WTAP knockdown group, while TEX41 was upregulated in the WTAP knockdown group (Fig. 7B and E). Also, IHC analysis demonstrated that HDAC1 was downregulated in the WTAP knockdown group (Fig. 7F). Moreover, tail vein metastasis model was performed to explore the role of WTAP on RCC metastasis in vivo. The result showed that silencing of WTAP significantly restrained the metastatic ability of 769-P cells in vivo (Fig. 7G). All together, these data reveal that WTAP knockdown inhibits RCC progression in vivo.

Discussion

Since m^6A modification could regulate gene expression in post-transcriptional levels, more and more studies have revealed that m^6A modification plays an important role in the development of tumors[26,27]. For example, METTL3 restrained tumor immune surveillance via regulating PD-L1 mRNA m^6A modification[28]. Similarly, Chen et al. reported that WTAP promotes liver cancer progression through the post-transcriptional suppression of ETS1 [29]. In RCC, Tang et al. revealed that WTAP promoted RCC proliferation by stabilizing CDK2 mRNA stability[29]. However, the role of WTAP in RCC metastasis has not been well studied. Our study indicated that WTAP was upregulated in RCC tissues compared to normal tissues. Also, RCC cell lines exhibited higher WTAP expression than normal renal epithelial cell line. Functional studies demonstrated that WTAP promoted RCC cell proliferation and metastasis.

Previous studies have shown that m^6A modification could regulate the stability, splicing, translocation, and translation of mRNA to regulate tumor progression[30]. For example, m^6A demethylase ALKBH5 could stabilize GLUT4 mRNA to promote breast cancer progression by decreasing its m^6A modification level[31]. However, not only mRNA, m^6A modification has been found enriched in tRNA, rRNA, and ncRNA[32,33]. Li et al. reported that WTAP could promote nasopharyngeal carcinoma progression by increasing lncRNA DIAPH1-AS1 m^6A

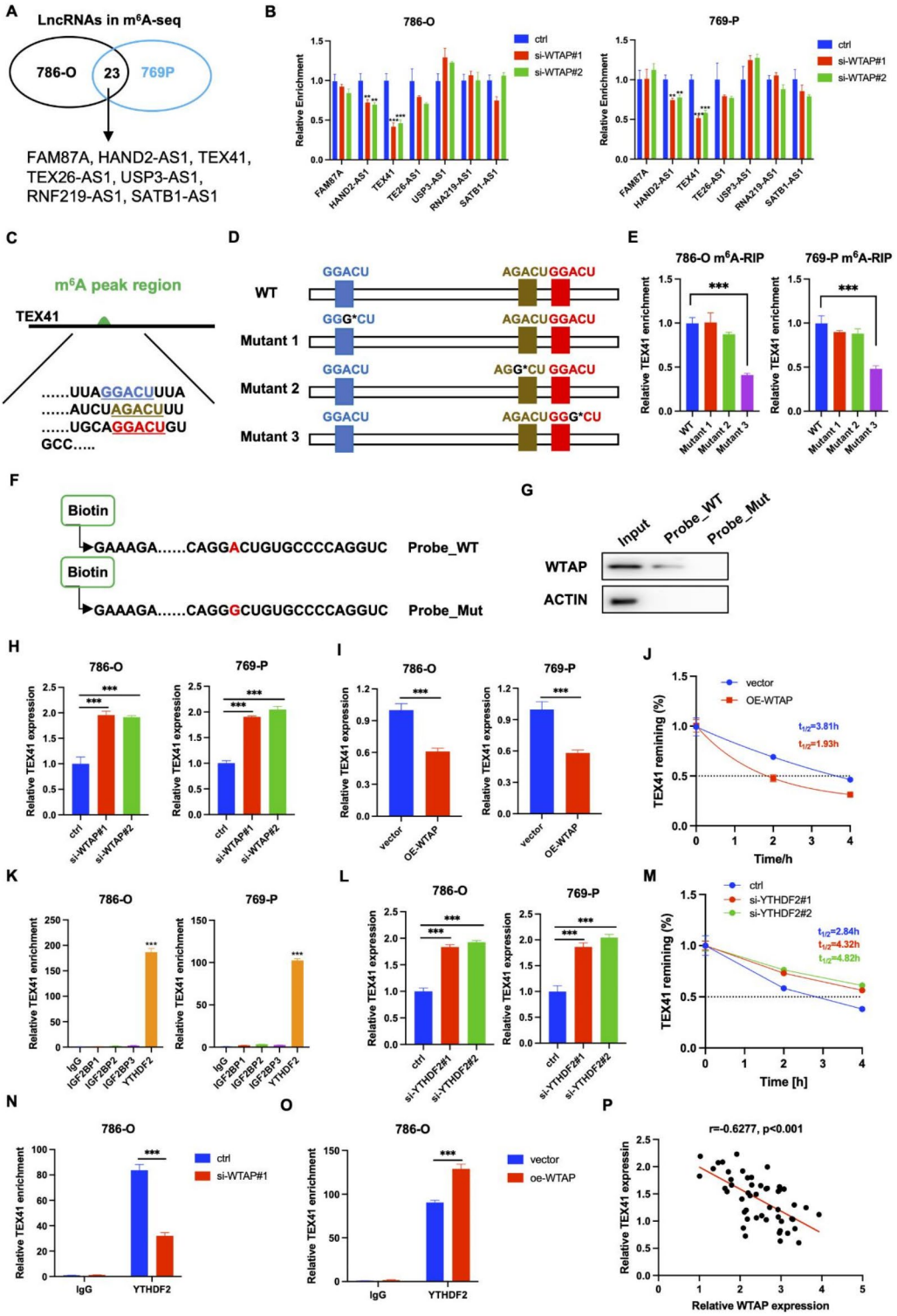

modification and stability[16]. To identified the WTAP-regulated lncRNAs in RCC, MeRIP-seq was performed in RCC cells with WTAP stable knockdown, and lncRNA TEX41 was identified. Further studies revealed that 4336 A was the critic m^{6}A site of TEX41. What's more, m^{6}A-modified TEX41 decreased its half-time in an YTHDF2-dependent manner.

LncRNA TEX41 has been reported to be dysregulated in several types of carcinoma. Zheng et al. showed that TEX41 promoted melanoma progression by regulating miR-103a-3p and C1QB expression[17]. Another group revealed that TEX41 accelerated acute lymphoblastic leukemia progression through reducing p53 and p21 expression[34]. However, the role of TEX41 in RCC is still unclear. In our study, we found that TEX41 was downregulated in RCC tissues compared to normal tissues. Functional assays indicated that TEX41 inhibited RCC progression. LncRNAs could bind with RNA, DNA, and proteins to regulate target genes expression. Previous studies revealed that TEX41 could serve as a miRNA sponge to regulate gene expression[35,36]. By using

◀**Fig. 3**. WTAP destabilized lncRNA TEX41 through YTHDF2 in an m^{6}A-dependent manner. (**A**) Venn diagram showed 23 hypomethylated lncRNAs using MeRIP-seq with WTAP knockdown. (**B**) m^{6}A-RIP assay validated the m^{6}A level of lncRNA selected from the MeRIP-seq. (**C**) The m^{6}A modification sites predicted by SRAMP database. (**D**) Diagram showed the TEX41 WT and three MUT plasmids used in the m^{6}A-RIP assay. (**E**) m^{6}A-RIP assay validated the m^{6}A modification site. (**F**) Schematic diagram showing the detailed information of probe_WT and probe_Mut. (**G**) RNA pulldown assay showed the binding capacity between probes and WTAP. (**H**) TEX41 expression was detected with WTAP knockdown. (**I**) TEX41 expression was detected with WTAP overexpression. (**J**) Half-time of TEX41 was detected in actinomycin D treated 786-O cells with WTAP overexpression or not. (**K**) Readers-RIP assay validated the m^{6}A reader which could recognize TEX41. (**L**) TEX41 expression was detected with YTHDF2 knockdown. (**M**) Half-time of TEX41 was detected in actinomycin D treated 786-O cells with YTHDF2 knockdown or not. (**N**) YTHDF2-RIP assay showed the binding capacity between TEX41 and YTHDF2 with WTAP knockdown or not. (**O**) YTHDF2-RIP assay showed the binding capacity between TEX41 and YTHDF2 with WTAP overexpression or not. (**P**) Correlation of WTAP and TEX41 in RCC tissues. The experiments were repeated three times independently. Data are presented as the mean ± SD. $^{**}P < 0.01$, $^{***}P < 0.001$.

online database, SUZ12 was identified as a TEX41-binding protein. Further studies revealed that TEX41 could enhance the histone methyltransferase activity of SUZ12 to silence downstream gene, HDAC1, expression.

H3K27me3 is a well-studied histone modification that plays a crucial role in gene regulation. Its presence at gene promoters leads to a more condensed chromatin state, repressing gene expression[37]. The enzyme complexes PRC2 and UTX/JMJD3 regulate H3K27me3 levels through methylation and demethylation, respectively[38]. Several studies have shown that decreased PRC2 activity and consequently lower H3K27me3 levels are associated with cancer progression[39]. Rogenhofer et al. found that RCC tissues exhibit lower H3K27me3 levels compared to normal tissues, and lower levels correlate with shorter progression-free survival[40]. In our study, we identified a novel mechanism contributing to low H3K27me3 levels in RCC cells. WTAP downregulates the enzyme activity of SUZ12, a key component of the PRC2 complex, by regulating the expression of the lncRNA TEX41. This ultimately leads to reduced H3K27me3 levels.

However, there are many areas in our research that can be further explored: (1) Insufficient clinical samples. We only explored the expression levels of WTAP in 50 pairs renal cancer tissues. Additionally, due to inadequate follow-up time, prognostic information is also lacking. In the future, we will continue to collect patient samples, gather clinical data, and validate the clinical significance of WTAP in a larger sample size. Also, many algorithms can be used to solve this problem[41,42]; (2) In the study of how TEX41 regulates SUZ12, we did not design corresponding truncations of SUZ12 to verify the specific binding sites of TEX41 with the SUZ12 protein, and how TEX41 actually influences the regulation of downstream HDAC1 by SUZ12; (3) The regulation of downstream genes by HDAC1 is quite extensive. In our upcoming research, we need to determine which part of the WTAP/TEX41/SUZ12 axis regulates the HDAC1 regulatory network.

In conclusion, our study proved that WTAP promoted RCC proliferation and metastasis in vivo and in vitro. MeRIP-seq revealed that the m^{6}A modification of lncRNA TEX41 was regulated by WTAP in an YTHDF2-dependent manner. Moreover, TEX41 could interact with SUZ12 and enhance its histone methyltransferase activity, resulting in HDAC1 silencing. Totally, our study exhibits a novel WTAP regulatory axis, which could be the potential therapeutic target for RCC treatment (Fig. 8).

Methods

MeRIP-seq

A total of RNA extracted from 786-O or 760-P transfected cells was incubated with m^{6}A-specific antibody. Then, the immunoprecipitated RNA was fragmented and reverse transcribed to cDNA. Moreover, the fragments were amplified with PCR and sequencingon an illumina Novaseq™ 6000. Finally, hypomethylated m^{6}A-methylated lncRNAs ($|\log_2 FC|>1$, $p < 0.05$) were selected.

Cell culture

RCC cell lines (786-O, 769-P, OSRC-2, and ACHN) and normal cell line HK-2 are obtained from Cell Resource Center, Chinese Academy of Sciences (Shanghai). RPMI-1640 medium (Gibco, USA) with 10% fetal bovine serum (Gibco, USA) are used for 786-O, 769-P, and OSRC-2 cells. HK-2 and ACHN were cultured in MEM medium (Gibco, USA) with 10% FBS.

SiRNAs and plasmids transfection

All siRNAs for WTAP, TEX41, and HDAC1 were designed and purchased from Genepharma (Shanghai). The detailed information of siRNAs was listed in the Supplementary Table S1. The jetPRIME reagent (Polyplus, Frence) was used for the transfection of siRNAs and plasmids.

RNA immunoprecipitation (RIP)

RIP assays were performed using Magna RIP RNA- Binding Protein Immunoprecipitation Kit (Millipore, USA). Briefly, 5ug m^{6}A, IGF2BP1, IGF2BP2, IGF2BP3, YTHDF2, or SUZ12 antibodies were conjugated to protein A/G magnetic beads 30 min at room temperature. Then, the antibodies/beads complex was incubated with cell lysate overnight at 4 °C. After washed for 5 times, the immunoprecipitated RNA was extracted and detected using RT-qPCR.

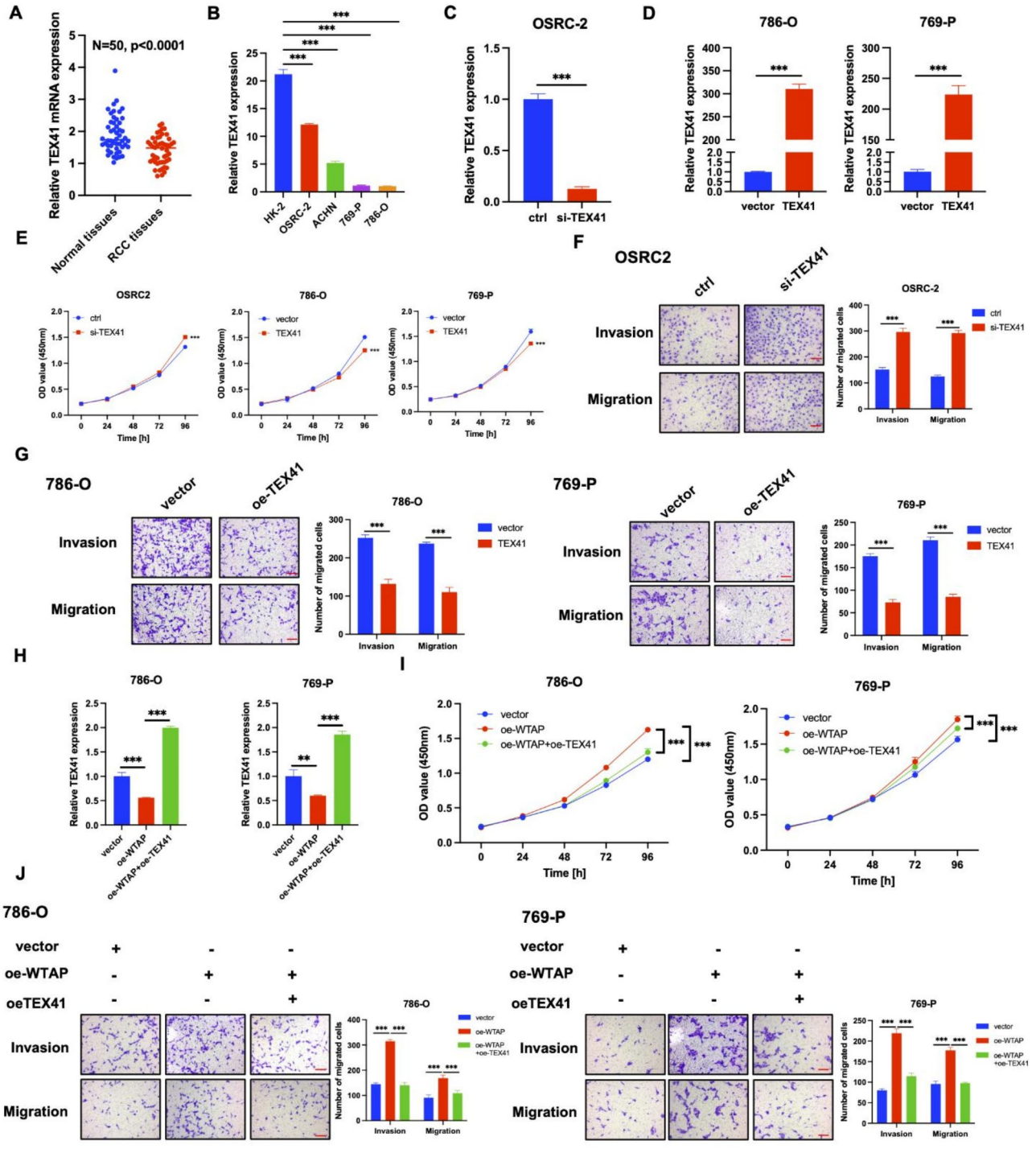

Fig. 4. LncRNA TEX41 restrained RCC cells proliferation and metastasis. (**A**) The relative expression of TEX41 in 50 paired RCC tissues. (**B**) The relative expression of TEX41 in RCC cell lines and normal cell line HK-2. (**C**) and (**D**) The knockdown (**C**) and overexpression (**D**) efficiency of TEX41 in RCC cells. (**E**) Cell proliferation was analyzed using CCK-8 assays with TEX41 knockdown or overexpression. (**F**) and (**G**) Cell metastatic ability was analyzed using transwell migration and invasion assay with WTAP knockdown (**F**) or overexpression (**G**). Scale bars, 5 μm. (**H**) The expression of TEX41 was detected in WTAP overexpression cells with TEX41 overexpression or not. (**I**) Cell proliferation was analyzed using CCK-8 assays in WTAP overexpression RCC cells with TEX41 overexpression or not. (**J**) Cell metastatic ability was analyzed using transwell assay in WTAP overexpression RCC cells with TEX41 overexpression or not. Scale bars, 5 μm. The experiments were repeated three times independently. Data are presented as the mean ± SD. $^{**}P < 0.01$, $^{***}P < 0.001$.

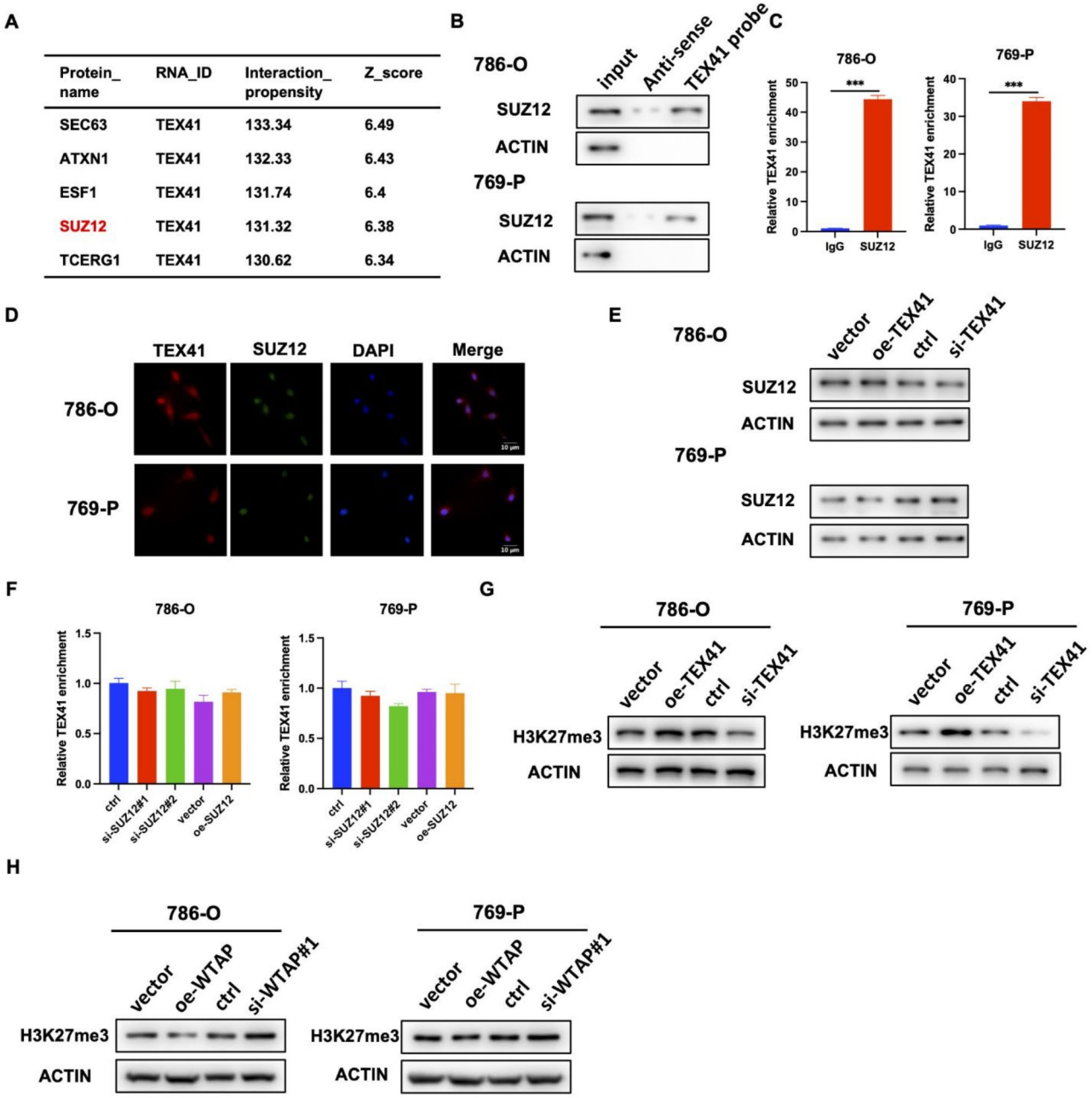

Fig. 5. TEX41 interacted with SUZ12 in RCC cells. (**A**) The table showed the TEX41-binding protein predicted using the catRAPID database. (**B**) RNA pull-down assay showed the interaction between TEX41 and SUZ12. (**C**) RIP assay showed the interaction between TEX41 and SUZ12. (**D**) FISH-IF assay showed the interaction between TEX41 and SUZ12, scale bar = 10 μm. (**E**) Western blotting assay showed the effect of TEX41 on SUZ12 expression. (**F**) RT-qPCT showed the effect of SUZ12 on TEX41 expression. (**G**) Western blotting assay showed the effect of TEX41 on cell total H3K27me3 level. (**H**) Western blotting assay showed the effect of WTAP on cell total H3K27me3 level. The experiments were repeated three times independently. Data are presented as the mean ± SD. $^{***}P < 0.001$.

Online database searching

To identify the expression pattern of WTAP in TCGA-KIRC database, we used UALCAN website (https://ualcan.path.uab.edu/index.html). In UALCAN database, we used the TCGA database, and chose clear cell renal cell carcinoma data to detected the WTAP expression in RCC tissues and normal tissues. To explore the correlation between HDAC1 and WTAP, we used GEPIA website (http://gepia.cancer-pku.cn/detail.php?gene). In GEPIA database, we used Correlation Analysis to detect the correlation between HDAC1 and WTAP in KIRC tumor tissues.

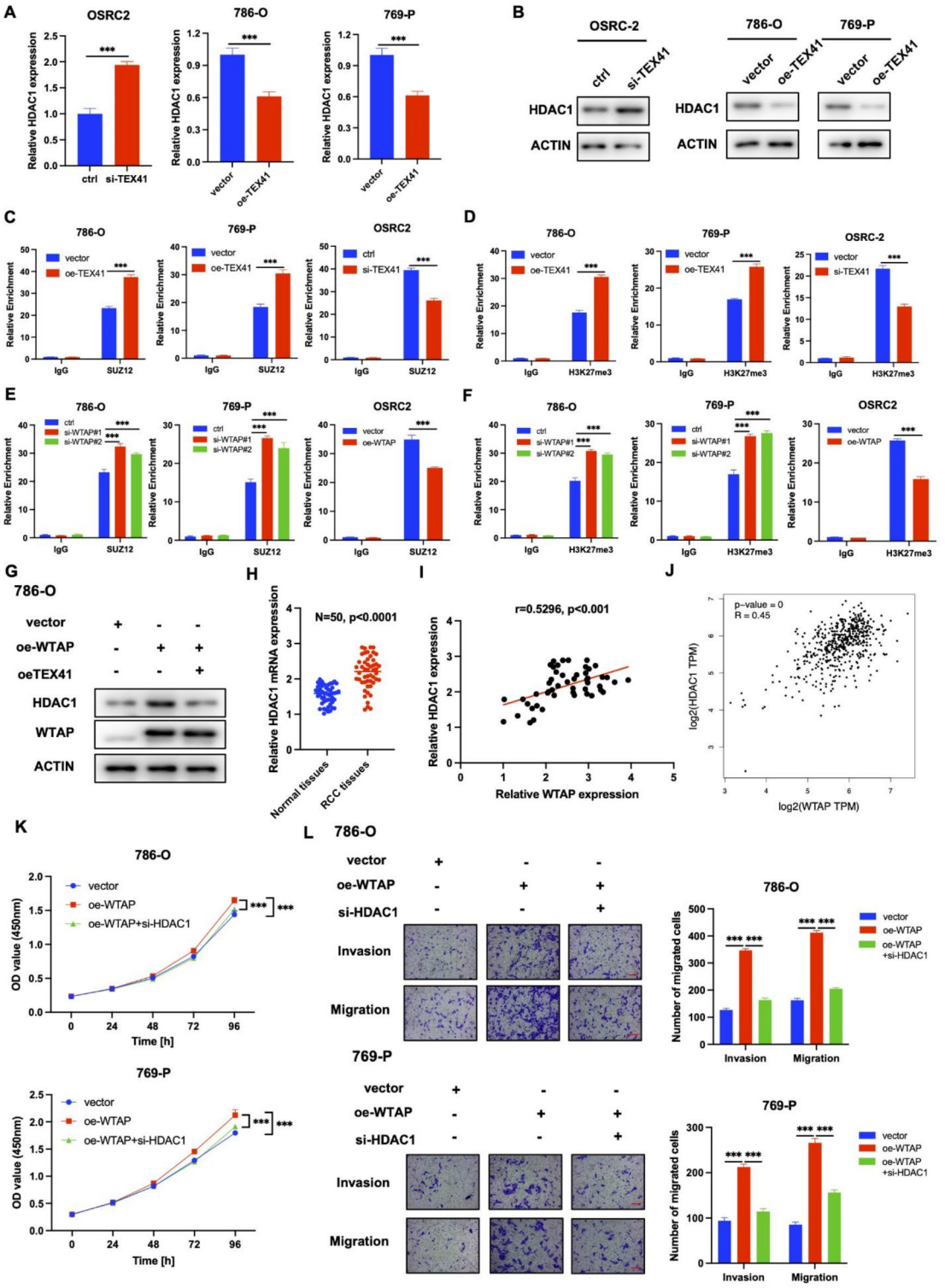

Immunohistochemistry assays

The RCC tissues and animal tissues were fixed in 4% paraformaldehyde for more than 24 h. Then, the tissue samples were embedded in paraffin and cut into 4 μm-thick sections, and incubated in 65 °C, companying with de-paraffinization. Then, 20 mM sodium citrate buffer was applied to retrieved the antigens at 80 °C for 15 min. After cooled down to the room temperature, 1% H2O2 were used to block the endogenous peroxidase activity for 15 min, followed by 5% goat serum to block the nonspecific binding sites for 30 min. Furthermore, the samples were incubated with anti-WTAP or anti-HDAC1 antibodies overnight at 4 °C. Next day, the samples were washed for three times and incubated with secondary antibody at room temperature, and were stained with diaminobenzidine tetrahydrochloride for 30s. The results were analyzed using the NPD software. According to the cell staining intensity, a score of 4 levels is assigned: no positive staining (negative) is scored as 0, light yellow (weakly positive) is scored as 1, brown-yellow (positive) is scored as 2, and brown (strongly positive) is scored as

◀**Fig. 6**. TEX41 modulated HDAC1 expression through regulating H3K27me3 level in its promotor region. (**A**) The mRNA expression of HDAC1 in RCC cells with TEX41 knockdown or overexpression. (**B**) The protein expression of HDAC1 in RCC cells with TEX41 knockdown or overexpression. (**C**) The impact of TEX41 overexpression or knockdown on the SUZ12 occupied at HDAC1 promotor in RCC cells. (**D**) The impact of TEX41 overexpression or knockdown on the H3K27me3 modification at HDAC1 promotor in RCC cells. (**E**) The impact of WTAP overexpression or knockdown on the SUZ12 occupied at HDAC1 promotor in RCC cells. (**F**) The impact of WTAP overexpression or knockdown on the H3K27me3 modification at HDAC1 promotor in RCC cells. (**G**) The expression of HDAC1 in WTAP overexpression cells with TEX41 overexpression or not. **H**, The relative expression of HDAC1 in 50 paired RCC tissues. (**I**) Correlation analysis of HDAC1 and WTAP in RCC tissues. (**J**) Correlation analysis of HDAC1 and WTAP based on the data from TCGA-KIRC database. (**K**) Cell proliferation was analyzed using CCK-8 in WTAP overexpression cells with HDAC1 knockdown or not. (**L**) Cell metastatic ability was analyzed using transwell assay in WTAP overexpression cells with HDAC1 knockdown or not. Scale bars, 5 μm. The experiments were repeated three times independently. Data are presented as the mean ± SD. $^{***}P < 0.001$.

3. Based on the percentage of positive cells, a score of 4 levels is assigned: ≤25% is scored as 1, 26-50% is scored as 2, 51-75% is scored as 3, and > 75% is scored as 4. The final score is obtained by multiplying the scores of these two assessments.

MeRIP-seq assays

MeRIP-seq was performed in duplicate on 786-O and 769-P cells with and without WTAP knockdown. Trizol reagent (Invitrogen, USA) was used for the isolation the RNA. Then, Dynabeads mRNA DIRECT Kit (Thermo Fisher) was applied to purified the obtained mRNA followed by sonication. Sonicated mRNA was mixed with m6A antibody (Synaptic Systems) in IP buffer and incubated under head-to-tail mixing at 4 °C for 2 h. Furthermore, the mixture was incubated with protein A magnetic beads (Thermo Fisher) at 4 °C for 2 h. After washed with IP buffer three times. m6A elution buffer was applied to elute mRNA two times. After purified by an RNA Clean and Concentrator (Zymo, Orange, CA), sequencing was carried out on the Illumina HiSeq 2000 system with pair-end 150-bp read length. Reads were aligned to human genome version 38 (GRCh38) with TopHat. The longest isoform was retained if a gene had more than one isoform. Differential m6A-modified peaks between IP and input samples were identified using exomePeak ($p < 0.01$).

RNA pulldown assay

The TEX41 and its antisense plasmids were used for the template for ex vivo synthesis of TEX41 and its antisense. Then, TEX41 and antisense were biotinylated. After incubated with streptavidin magnetic beads and cell lysate of 786-O and 769-P, the pulldown proteins were detected using western blotting.

Real-time quantitative PCR (RT-qPCR)

Trizol reagent (Invitrogen, USA) was used for the isolation the RNA. RNA was reverse-transcribed using HiScript III RT SuperMix (Vazyme, China). RT-qPCR was performed using LightCycler® 480 System (Roche, Switzerland) with qPCR kit (Takara, Japan). The primer information was listed in the Supplementary Table S2.

Western blotting

Cells and tissues were lysed using RIPA lysis buffer (Beyotime, China) containing proteinase inhibitor (Beyotime, China). Equal amounts of proteins were separated by 10% SDS-PAGE and then transferred to PVDF membrane (Bio-Rad). Membranes were incubated with primary antibodies overnight at 4 °C. The next day, the membrane was washed for 3 times and then incubated with secondary antibodies for an hour. Finally, the membrane was visualization using ChemiDoc Imaging Systems (Bio-Rad, USA). The antibodies information was listed in the Supplementary Table S3.

Clinical specimens

All clinical samples were obtained from Sir Run Run Shaw Hospital, School of Medicine, Zhejiang University. The Ethics Committee of Sir Run Run Shaw Hospital, School of Medicine, Zhejiang University have approved this study (SRRSH202102230). All of the experiments were complied with the ARRIVE guidelines (https://arriveguidelines.org). All the methods are performed in accordance with The Ethics Committee of Sir Run Run Shaw Hospital, School of Medicine, Zhejiang University' guidelines. The written informed consent was obtained from the patients.

CCK-8 assay

A total of $2*10^3$ transfected RCC cells were placed into 96-well plate. To detect the cell vitality, 100 uL complete medium containing 10% CCK-8 solution (Dojindo) were added to the well, the optical densities at 450 nm. The cell vitality was detected every 24 h for 5 days.

Transwell assays

For transwell assay, transwell chamber (Corning, USA) were placed with (for invasion assay) or without (for migration assay) Matrigel (Corning, USA) according to the the manufacturer's manual. 200 uL serum-free medium containing $3*10^4$ RCC cells (for migration assay) or $9*10^4$ RCC cells (for invasion assay) in were placed into the upper chamber. The lower chamber was placed with medium wtih 10% FBS. After 24 h, the chamber

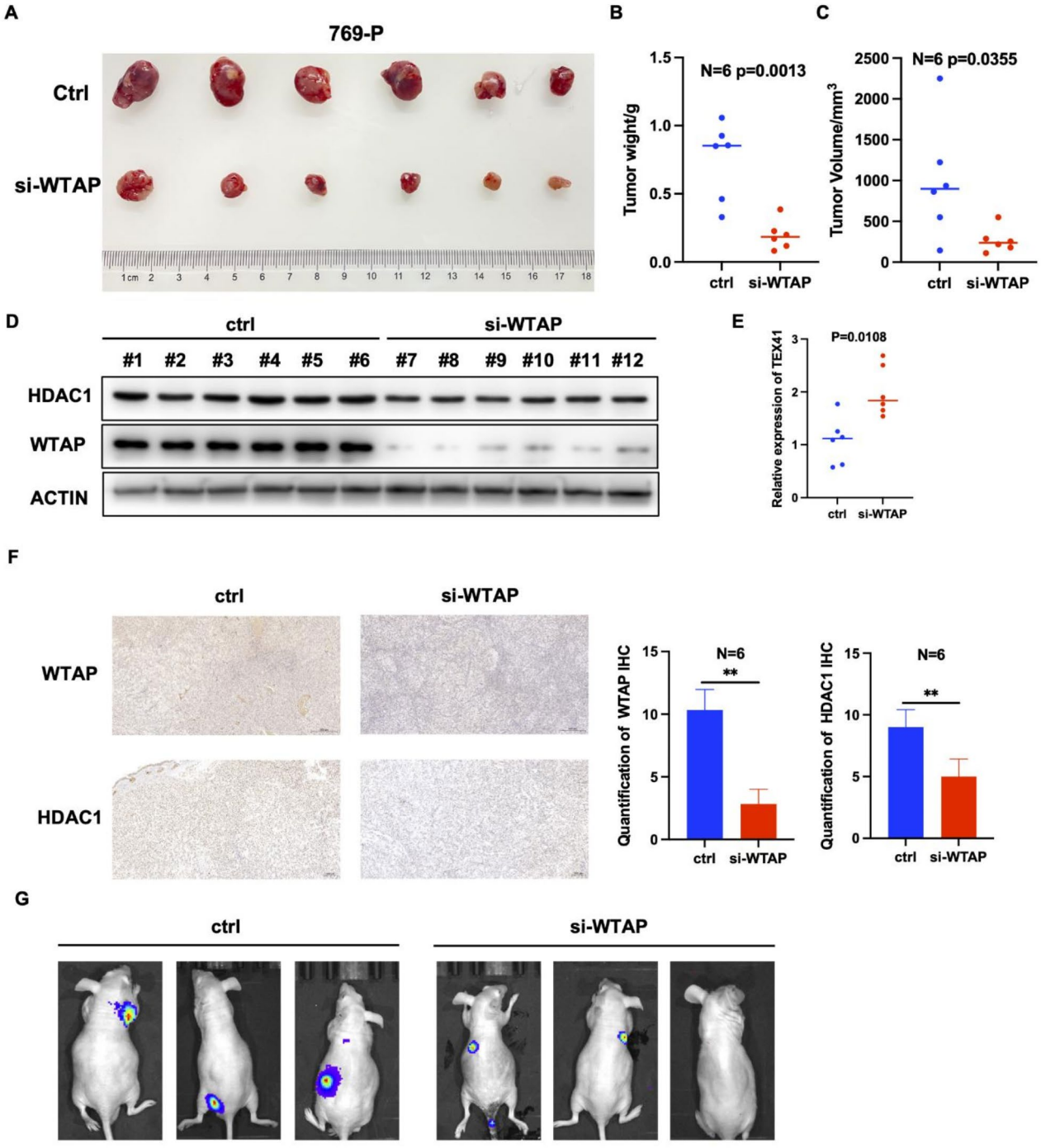

Fig. 7. Silencing of WTAP restrained RCC progression in vivo. (**A**) Representative image of the xenograft tumors in control and WTAP knockdown groups. (**B**, **C**) Tumor weight (**B**) and tumor volume (**C**) were evaluated in control and WTAP knockdown groups. (**D**) The relative expression of WTAP and HDAC1 were evaluated in control and WTAP knockdown groups. (**E**) The relative expression of TEX41 was evaluated in control and WTAP knockdown groups. (**F**) IHC analysis showed the expression of WTAP and HDAC1. The experiments were repeated three times independently. G, Tail vein metastasis model showing the metastatic ability of 769-P cells in control and WTAP knockdown groups. Data are presented as the mean ± SD. $^{**}P < 0.01$.

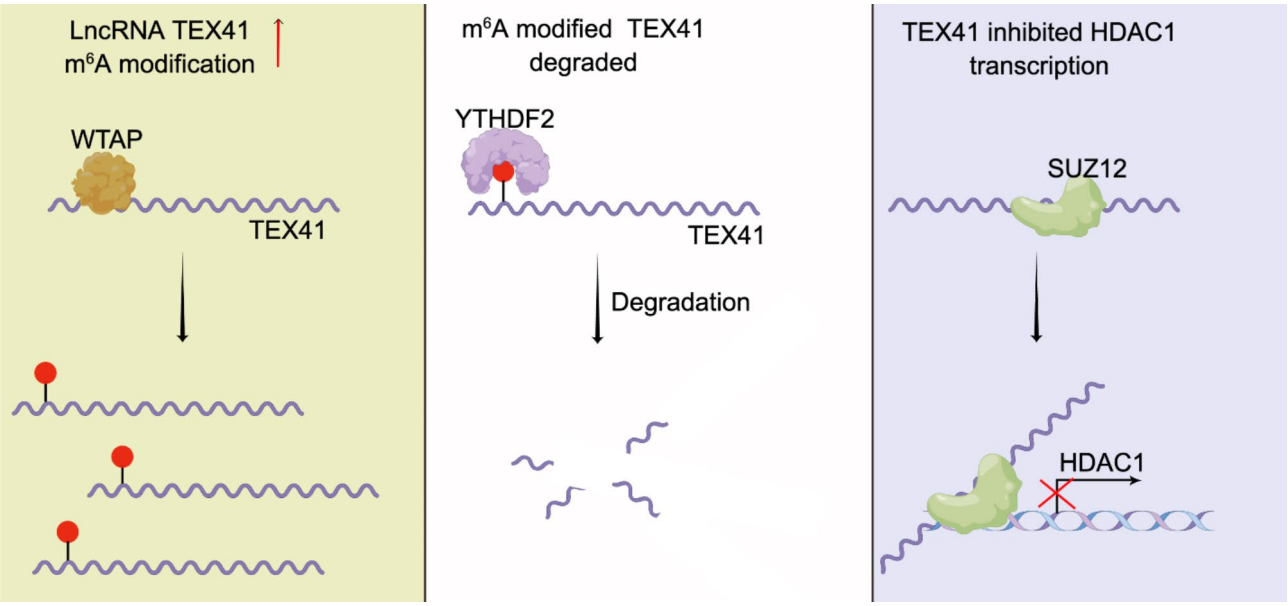

Fig. 8. The schematic diagram illustrating the role of WTAP in renal cell carcinoma. In RCC cells, WTAP introduced m6A modifications in the LncRNA TEX41, leading to the degradation of TEX41 in a YTHDF2-dependent manner. Furthermore, TEX41 was found to interact with SUZ12, enhancing its histone methyltransferase activity and consequently silencing HDAC1.

was fixed for 20 min and stained with 0.2% crystal violet for 15 min. Then, the migrated cells were photographed and counted.

Colony formation assay

A total of 1000 transfected RCC cells were plated into a well of 6-well plate for 2 weeks and changed the fresh medium every 4 days. 2 weeks later, cells were fixed, dyed with crystal violet (Beyotime, China) and photographed.

Cell cycle and apoptosis assay

For cell cycle assays, Cell Cycle Staining Kit (BD Biosciences, USA) was applied. Briefly, more than $1*10^5$ transfected RCC cells were collected and incubated with PI for 30 min. Then, the cell cycle was detected using a flow cytometer.

For apoptosis assays, Annexin V-FITC/PI Apoptosis Kit (BD Biosciences, USA) was applied. Briefly, more than $1*10^5$ transfected RCC cells were collected and incubated with Annexin V-FITC and PI for 15 min. Then, the apoptosis rate was detected using a flow cytometer.

Animal experiments

All of the following experiments reported in accordance with ARRIVE guidelines (https://arriveguidelines.org). All the experiment protocol was approved by Ethics Committee of Sir Run Run Shaw Hospital, School of Medicine, Zhejiang University (SRRSH202102230).

For xenograft mice model, $1*10^6$ 769-P stably transfected cells were subcutaneously injected into the 4-weeks nude mice. After 5 weeks, the mice were anesthetized by intraperitoneal injection of pentobarbital and then sacrificed by dissection, and the tumor were measured. Then, the tumors were extracted for RNA and protein for further detection.

For tail vein mice metastasis model, $2*10^6$ 769-P stably transfected cells were injected into the 4-weeks nude mice via tail vein. After 4 weeks, all mice were photographed using in vivo imaging system. Finally, the mice were anesthetized by intraperitoneal injection of pentobarbital and then sacrificed.

Chromatin immunoprecipitation (ChIP)

ChIP assays were performed using Pierce Magnetic ChIP Kit (Thermo Fisher Scientific, USA). About $4*10^6$ transfected RCC cells were treated with 1% formaldehyde and followed by glycine. The the sonicated DNA (~200–500 bp) was incubated with IgG, SUZ12, or H3K27me3 antibodies. After washed with 3 times low salt solution and 1 time high salt solution, the immunoprecipitated DNA was extracted and detected using qPCR.

Statistics

GraphPad Prism (version 8.0, GraphPad Software, Inc.) was used for Statistical analyses. The difference between the two groups using student's t-test. And the different between multiple groups using one-way ANOVA. *P* value less than 0.05 was considered as statistically significant.

Data availability

The datasets used and/or analyzed during the current study are available within the manuscript and its supplementary information files.

Received: 12 August 2024; Accepted: 14 October 2024
Published online: 21 October 2024

References

1. Siegel, R. L., Miller, K. D. & Jemal, A. Cancer statistics, 2019. *CA Cancer J. Clin.* **69**, 7–34 (2019).
2. Linehan, W. M. & Ricketts, C. J. The Cancer Genome Atlas of renal cell carcinoma: findings and clinical implications. *Nat. Rev. Urol.* **16**, 539–552 (2019).
3. Pontes, O., Oliveira-Pinto, S., Baltazar, F. & Costa, M. Renal cell carcinoma therapy: current and new drug candidates. *Drug Discov Today*. **27**, 304–314 (2022).
4. Jonasch, E., Walker, C. L. & Rathmell, W. K. Clear cell renal cell carcinoma ontogeny and mechanisms of lethality. *Nat. Rev. Nephrol.* **17**, 245–261 (2021).
5. Bukavina, L. et al. Epidemiology of renal cell carcinoma: 2022 update. *Eur. Urol.* **82**, 529–542 (2022).
6. Molina-Cerrillo, J. et al. Epigenetics in advanced renal cell carcinoma: potential new targets. *Crit. Rev. Oncol. Hematol.* **180**, 103857 (2022).
7. Zhao, B. S., Roundtree, I. A. & He, C. Post-transcriptional gene regulation by mRNA modifications. *Nat. Rev. Mol. Cell. Biol.* **18**, 31–42 (2017).
8. Jiang, X. et al. The role of m6A modification in the biological functions and diseases. *Signal. Transduct. Target. Ther.* **6**, 74 (2021).
9. Shi, H., Wei, J. & He, C. Where, when, and how: context-dependent functions of RNA methylation writers, readers, and Erasers. *Mol. Cell.* **74**, 640–650 (2019).
10. Ni, W. J. et al. RNA N6 -methyladenosine modifications and potential targeted therapeutic strategies in kidney disease. *Br. J. Pharmacol.* **180**, 5–24 (2023).
11. Zhu, D. et al. The methyltransferase METTL3 promotes tumorigenesis via mediating HHLA2 mRNA m6A modification in human renal cell carcinoma. *J. Transl Med.* **20**, 298 (2022).
12. Tang, J. et al. Wilms' tumor 1-associating protein promotes renal cell carcinoma proliferation by regulating CDK2 mRNA stability. *J. Exp. Clin. Cancer Res.* **37**, 40 (2018).
13. Zhang, C. et al. Downregulated METTL14 accumulates BPTF that reinforces super-enhancers and distal lung metastasis via glycolytic reprogramming in renal cell carcinoma. *Theranostics.* **11**, 3676–3693 (2021).
14. Xu, Y. et al. FTO-mediated autophagy promotes progression of clear cell renal cell carcinoma via regulating SIK2 mRNA stability. *Int. J. Biol. Sci.* **18**, 5943–5962 (2022).
15. Fang, Z. et al. Role of m6A writers, erasers and readers in cancer. *Exp. Hematol. Oncol.* **11**, 45 (2022).
16. Zheng, Y. et al. IRF4-activated TEX41 promotes the malignant behaviors of melanoma cells by targeting miR-103a-3p/C1QB axis. *BMC Cancer*. **21**, 1339 (2021).
17. Orlandella, F. M. et al. The lncRNA TEX41 is upregulated in pediatric B-Cells Acute Lymphoblastic Leukemia and it is necessary for leukemic cell growth. *Biomark. Res.* **9**, 54 (2021).
18. Yu, J. R., Lee, C. H., Oksuz, O., Stafford, J. M. & Reinberg, D. PRC2 is high maintenance. *Genes Dev.* **33**, 903–935 (2019).
19. Laugesen, A., Højfeldt, J. W. & Helin, K. Molecular mechanisms directing PRC2 recruitment and H3K27 methylation. *Mol. Cell.* **74**, 8–18 (2019).
20. Jiang, M. et al. MARCKSL1-2 reverses docetaxel-resistance of lung adenocarcinoma cells by recruiting SUZ12 to suppress HDAC1 and elevate miR-200b. *Mol. Cancer.* **21**, 150 (2022).
21. Dunaway, L. S. & Pollock, J. S. HDAC1: an environmental sensor regulating endothelial function. *Cardiovasc. Res.* **118**, 1885–1903 (2022).
22. Wang, Y. & Wang, H. The emerging role of histone deacetylase 1 in allergic diseases. *Front. Immunol.* **13**, 1027403 (2022).
23. Willis-Martinez, D., Richards, H. W., Timchenko, N. A. & Medrano, E. E. Role of HDAC1 in senescence, aging, and cancer. *Exp. Gerontol.* **45**, 279–285 (2010).
24. Kiweler, N. et al. The histone deacetylases HDAC1 and HDAC2 are required for the growth and survival of renal carcinoma cells. *Arch. Toxicol.* **92**, 2227–2243 (2018).
25. Ramakrishnan, S. et al. HDAC 1 and 6 modulate cell invasion and migration in clear cell renal cell carcinoma. *BMC Cancer*. **16**, 617 (2016).
26. Roundtree, I. A., Evans, M. E., Pan, T. & He, C. Dynamic RNA modifications in Gene expression regulation. *Cell.* **169**, 1187–1200 (2017).
27. Wang, X. et al. N(6)-methyladenosine modulates Messenger RNA translation efficiency. *Cell.* **161**, 1388–1399 (2015).
28. Wan, W. et al. METTL3/IGF2BP3 axis inhibits tumor immune surveillance by upregulating N6-methyladenosine modification of PD-L1 mRNA in breast cancer. *Mol. Cancer*. **21**, 60 (2022).
29. Chen, Y. et al. WTAP facilitates progression of hepatocellular carcinoma via m6A-HuR-dependent epigenetic silencing of ETS1. *Mol. Cancer*. **18**, 127 (2019).
30. Fu, Y., Dominissini, D., Rechavi, G. & He, C. Gene expression regulation mediated through reversible m^6A RNA methylation. *Nat. Rev. Genet.* **15**, 293–306 (2014).
31. Liu, H. et al. ALKBH5-Mediated m6A demethylation of GLUT4 mRNA promotes glycolysis and resistance to HER2-Targeted therapy in breast Cancer. *Cancer Res.* **82**, 3974–3986 (2022).
32. Ma, S. et al. The interplay between m6A RNA methylation and noncoding RNA in cancer. *J. Hematol. Oncol.* **12**, 121 (2019).
33. Chen, C. et al. m6A modification in non-coding RNA: the role in Cancer Drug Resistance. *Front. Oncol.* **11**, 746789 (2021).
34. Li, Z. X. et al. WTAP-mediated m6A modification of lncRNA DIAPH1-AS1 enhances its stability to facilitate nasopharyngeal carcinoma growth and metastasis. *Cell. Death Differ.* **29**, 1137–1151 (2022).
35. Peng, W. X., Koirala, P. & Mo, Y. Y. LncRNA-mediated regulation of cell signaling in cancer. *Oncogene*. **36**, 5661–5667 (2017).
36. Bhan, A., Soleimani, M. & Mandal, S. S. Long noncoding RNA and Cancer: a New Paradigm. *Cancer Res.* **77**, 3965–3981 (2017).
37. Margueron, R. & Reinberg, D. The polycomb complex PRC2 and its mark in life. *Nature*. **469**, 343–349 (2011).
38. Suvà, M. L., Riggi, N. & Bernstein, B. E. Epigenetic reprogramming in cancer. *Science*. **339**, 1567–1570 (2013).
39. Conway, E., Healy, E. & Bracken, A. P. PRC2 mediated H3K27 methylations in cellular identity and cancer. *Curr. Opin. Cell. Biol.* **37**, 42–48 (2015).
40. Rogenhofer, S. et al. Global histone H3 lysine 27 (H3K27) methylation levels and their prognostic relevance in renal cell carcinoma. *BJU Int.* **109**, 459–465 (2012).
41. Tang, Y., Huang, J., Pedrycz, W., Li, B. & Ren, F. A fuzzy clustering validity Index Induced by Triple Center Relation. *IEEE Trans. Cybern.* **53**, 5024–5036 (2023).
42. Tang, Y., Pan, Z., Hu, X., Pedrycz, W. & Chen, R. Knowledge-Induced multiple Kernel fuzzy clustering. *IEEE Trans. Pattern Anal. Mach. Intell.* **45**, 14838–14855 (2023).

Author contributions

GL and LX, Conceptualization, Supervision, and Validation; ZZ and XC, Data curation, Methodology, Software, Visualization, Writing – original draft; HW, LD, and MW, Data curation, Software, Validation. All authors have agreed to publish this manuscript.

Funding

This work was supported by National Natural Science Foundation of China (Grant Numbers: 82472720, 82372687, 82103242, 82072809); Joint construction project of Zhejiang Province and Ministry (grant number: 2020388200); Key R & D plan of Zhejiang Province (grant number: 2019C03089); Natural Science Foundation of Zhejiang Province (LY22H160009).

Declarations

Competing interests

The authors declare no competing interests.

Ethic approval and consent to participate

This study was approved by the Ethics Committee of Sir Run Run Shaw Hospital, School of Medicine, Zhejiang University. All the methods are performed in accordance with The Ethics Committee of Sir Run Run Shaw Hospital, School of Medicine, Zhejiang University' guidelines.

Additional information

Supplementary Information The online version contains supplementary material available at https://doi.org/10.1038/s41598-024-76326-9.

Correspondence and requests for materials should be addressed to G.L. or L.X.